

High-resolution ion time-of-flight analysis for measuring molecular velocity distributions

Y. Kim, S. Ansari, B. Zwickl, and H. Meyer^{a)}

Department of Physics and Astronomy, The University of Georgia, Athens, Georgia 30602-2451

(Received 16 May 2003; accepted 31 August 2003)

A new electrode setup for high-resolution ion time-of-flight (TOF) analysis is described. The setup is used in combination with a counterpropagating pulsed molecular-beam scattering apparatus and laser ionization to measure one-dimensional velocity distributions of low-energy molecular products resulting from scattering or dissociation processes. In the case of ensembles characterized by cylindrical symmetry with respect to the molecular-beam axis, measured TOF spectra represent the angular distribution of the products. In the imaging of the ions onto the detector, this symmetry is preserved by using a pair of electrostatic mirrors for the deflection. Combined with separate velocity dispersion and acceleration fields, the present arrangement achieves superior resolution and detection efficiency. Although the resolution of the setup is limited by the velocity distribution of the molecular-beam pulses, changes in the average local velocity as small as 10 m/s have been observed. © 2003 American Institute of Physics. [DOI: 10.1063/1.1621061]

I. INTRODUCTION

Molecular-beam techniques are extremely powerful tools for the experimental study of the molecular reaction dynamics.¹ One of the ultimate goals in these experiments is the quantum state specific detection of products from processes like photodissociation, bimolecular reactions, or surface scattering.² Over the past decade, great progress has been made in achieving this goal including the measurement of state resolved differential cross sections and alignment moments.³

While quantum state specific information is usually obtained by means of laser spectroscopic detection, several techniques directly derive information on quantum states by measuring the kinetic energy of the products. Because of its sensitivity, the method of Rydberg tagging of H atoms provides very detailed angle and state information.^{4,5} Alternatively, information on the angular distribution of the products is obtained through methods based on the Doppler effect.^{6–8} Quantum state resolved velocity distributions are obtained from a measured Doppler profile of a suitable resonance line. A similar approach is based on resonance enhanced multiphoton ionization (REMPI) schemes to generate product ions which are subjected to different electrostatic fields in order to disperse different velocity groups. In the method of two-dimensional ion imaging, the velocity projection perpendicular to the dispersing field is measured.^{9–12} Alternatively, the method of ion time-of-flight (TOF) analysis provides information on the velocity component parallel to the dispersing field.^{13–15}

In the past, we have developed the method of counterpropagating pulsed molecular-beam scattering.^{16,17} The method combines sensitive REMPI detection with ion TOF analysis to measure state resolved differential cross sections

as well as differential moments of the collision-induced alignment. In principle, the method can be applied to any molecular process resulting in a product ensemble with cylindrical symmetry around the molecular-beam axis. In the original design, we used a single electrostatic mirror to deflect the ions off the molecular-beam axis toward the detector. Because the mirror breaks the cylindrical symmetry of the ion imaging arrangement, ions with a large off-axis velocity component have a TOF which depends on the azimuthal angle around the field direction.

In this article, we report two significant improvements of the previous setup: (1) The introduction of a second electrostatic mirror preserves the cylindrical symmetry for the ion TOF analysis, and (2) The use of separate fields for the velocity dispersion and ion acceleration results in a greatly improved velocity resolution while maintaining a high detection sensitivity. The new electrode setup is tested for the scattering of NO from Ne.

II. EXPERIMENTAL DETAILS

Details of the molecular-beam apparatus have been described previously.^{16,17} Briefly, two pulsed molecular-beam sources are mounted in a 500 mm diameter source chamber pumped by an 11 000 1/s diffusion pump. This chamber also contains the differentially pumped scattering chamber evacuated by a 3000 1/s diffusion pump. Both diffusion pumps are backed by a single roots-rotary pump combination. The molecular-beam pulses enter the scattering chamber through skimmers on opposite walls of the scattering chamber. The laser system employed is a Nd:YAG pumped dye laser whose output frequency is doubled in a KDP crystal. The resulting UV radiation is focused onto the molecular-beam axis with a 500 mm lens. Pulse energies of about 1 mJ are used for the detection of scattered NO molecules via (2+1) REMPI.

^{a)}Electronic mail: hmeyer@hal.physast.uga.edu

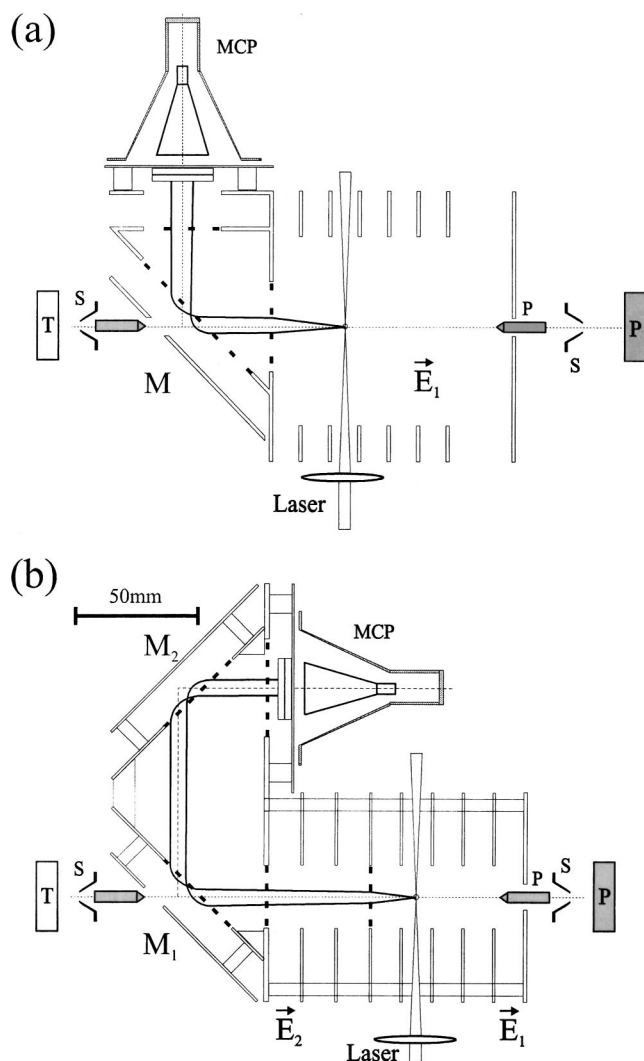


FIG. 1. (a) Original electrode arrangement described in detail (in Ref. 17). Ions are accelerated for 40 mm and drift over an effective distance of about 75 mm. The latter distance includes travel through the mirror. (b) Vertical cut through the electrode arrangement for the ion TOF analysis using two electrostatic mirrors, M_1 and M_2 . The setup allows for the use of two separate electric fields for velocity dispersion (E_1) and acceleration (E_2). Molecular-beam sources are labeled T (target beam) and P (primary beam). Molecular-beam pulses pass through skimmers (S) into the scattering chamber. Ions generated at the laser crossing move through the different electric fields (60 mm) until they reach the microchannel plate detector (MCP) after passing through an effective field free region of about 130 mm.

Figure 1 shows a schematics of the two different electrode arrangements used for the ion TOF analysis. In the original design [see (a) in Fig. 1], ions generated by the focused laser beam were subjected to a single constant homogeneous electric field.¹⁷ In order to achieve sufficient velocity dispersion, the field strength was limited to values of only a few V/cm resulting in long ion flight times. Because the ions were deflected off the molecular-beam axis toward the microchannel plate (MCP) detector (Del Mar Ventures, San Diego, CA) using a single electrostatic mirror, the mirror introduced a serious distortion of the TOF for ions with different directions of the off-axis velocity component. A quantitative measure of this distortion is determined by calculating arrival times for ion trajectories with the same initial position but different initial velocities assuming constant

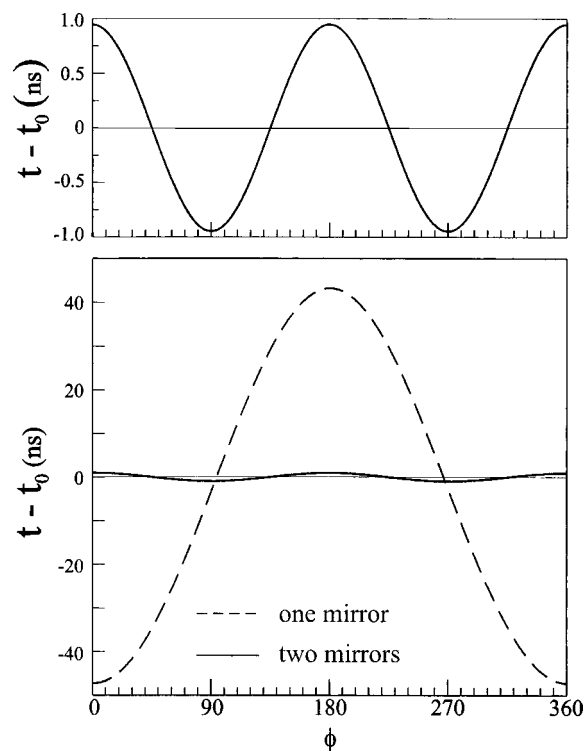


FIG. 2. Dependence of the NO^+ TOF on the azimuthal angle ϕ for the one- and two-mirror setups displayed in Fig. 1 in combination with a single dispersion field of 5.8 V/cm and mirror fields of 25 V/cm and 38 V/cm, respectively. Arrival times are calculated assuming constant fields in each region of the respective setup.

electric fields for each region of the respective setup. As the dashed curve in Fig. 2 demonstrates for NO^+ , the arrival time depends strongly on the azimuthal angle ϕ for a nonvanishing off-axis velocity component. Assuming a variation of the off-axis velocity component by ± 600 m/s, the calculated arrival time varies by about 100 ns for a dispersion field of 5.8 V/cm and a mirror field of 25 V/cm. For comparison, the same variation in the on-axis component results in a desired dispersion of about $0.7 \mu\text{s}$ (see Fig. 4). The reason for the aberration is illustrated in Fig. 3. In Fig. 3, we display two ion trajectories with opposite initial off-axis velocity components in the plane defined by the velocity dispersion field and the mirror normal. Figure 3 also schematically indicates the relevant velocity components and field directions at the entry of the trajectory into the mirror field. Trajectories having opposite initial off-axis velocity components enter the mirror with different angles with respect to the mirror field direction resulting in different residence times and thus a ϕ -dependent variation of the TOF. This situation is greatly improved by introducing an additional mirror which directly compensates for the aberration introduced by the first mirror. For example, if the off-axis velocity component makes a small angle with the mirror field upon entering the mirror, the same trajectory makes a large angle with the field direction of the second mirror. For the trajectory with the opposite initial off-axis velocity component, the situation upon entering the two-mirror fields is reversed. As shown in Fig. 2 as the solid curve, the dependence of the TOF on the azimuthal angle is effectively removed. The enlargement in the top part of Fig. 2 shows that the remaining variation is limited to less than ± 1

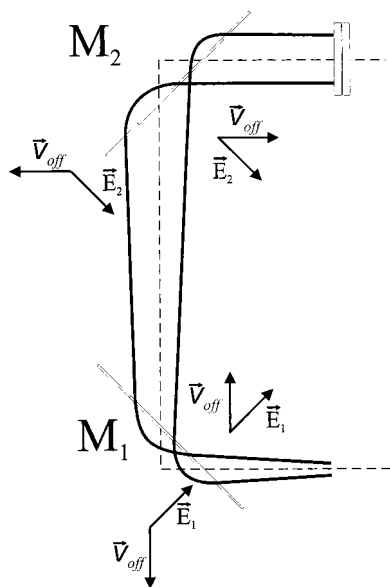


FIG. 3. Ion trajectories for the two-mirror setup.

ns. From Fig. 2, it is also evident that the remaining aberration is of second order, i.e., it is proportional to $\cos 2\phi$. As a result, the combination of two mirrors preserves the cylindrical symmetry of the setup.

Because of the counterpropagating beam setup, we have at our disposal two independent molecular-beam sources allowing the generation of ensembles with very different average velocity projections. We test the overall velocity dispersion capability of an electrode arrangement by expanding identical gas mixtures from both beam sources. The resulting molecular-beam pulses represent ensembles characterized by opposite average velocity projections in the direction of the dispersion field. As shown in the upper part of Fig. 4, first

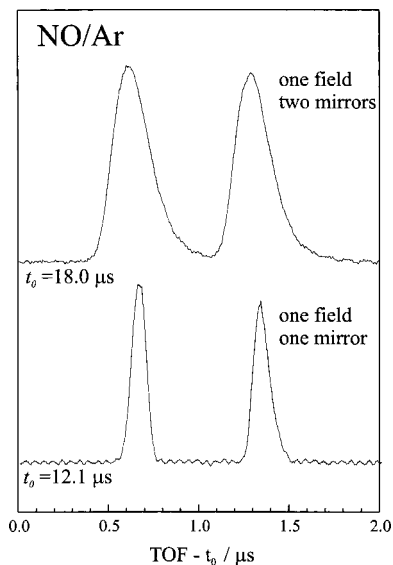


FIG. 4. TOF spectra of NO^+ with both molecular-beam sources operating with a mixture of 5% NO in Ar. In both cases, a single electric field is used for velocity dispersion and ion acceleration. The bottom spectrum is taken with the original one-mirror arrangement using (2+1) REMPI via the NO E state: Dispersion field 5.8 V/cm, mirror field 25 V/cm. The top spectrum is recorded in the two-mirror setup using (1+1) REMPI via the NO A state: Dispersion field 5.8 V/cm, mirror fields 38 V/cm.

tests of a setup involving two identical electrostatic mirrors resulted in significantly broadened ion peaks most likely caused by ion-ion repulsion due to larger ion densities in the case of (1+1) REMPI detection of NO via the A state. In comparison with the one-mirror arrangement, the overall TOF for the two-mirror version increased by 50% allowing the Coulomb distortion to cause additional broadening. Because of limitations in detection efficiency, it was not possible to fully recover the theoretical resolution by reducing the laser pulse energy.

This unsatisfactory situation is greatly improved by using a two-field arrangement consisting of a weak velocity dispersion field followed by a strong acceleration field. The schematic of this electrode arrangement is shown in Fig. 1 part (b). The velocity dispersion and the acceleration fields are defined by 5 and 4 stainless-steel electrodes (85 mm \times 85 mm \times 1 mm) with spacings of 11.6 mm and 13.0 mm, respectively. All electrodes have a 25 mm diameter hole except for the entrance electrode which has a 10 mm hole in order to further collimate the molecular beam. The two fields are separated by a Ni wire mesh (95% transmission, 20 lines/in., Buckbee Mears, Cortland, NY). In order to prevent interference due to backscattering of molecules of the primary molecular-beam pulse from the wire mesh, the scattering and laser detection regions are located 20 mm upstream of the wire mesh. The different electrodes are connected with precision resistors: 1.2 M Ω (dispersion field) and 1.0 M Ω (acceleration field). The reflectors are formed by spacing two stainless-steel electrodes 13 mm apart (entrance electrodes: 87 mm \times 85 mm \times 1 mm, back electrodes: 85 mm \times 85 mm \times 1 mm). The entrance electrodes have elliptically shaped holes (semiaxes: 12.7 mm and 25.5 mm) covered with Ni wire mesh (95% transmission, 20 lines/in., Buckbee Mears). The lower back electrode is equipped with a small hole of elliptical shape (semiaxes: 3.5 mm and 6.0 mm) to allow passage for the target molecular-beam pulse. In the velocity dispersion mode, separate voltages are applied to the first electrode of each field. Typically, we use fields of 4.5 V/cm for the velocity dispersion field, 72 V/cm for the acceleration field, and 460 V/cm for the mirror fields.

The velocity dispersion properties of the setup can be analyzed by considering a linear two-field arrangement followed by a field free drift region of effective length D_3 which takes into account the distance travelled through the mirror fields. If the two-field regions are of length D_1 and D_2 with field strength E_1 and E_2 , respectively, the ion TOF for this setup will be given by

$$T = -\frac{v_z}{\beta_1} + v_1 \left(\frac{1}{\beta_1} - \frac{1}{\beta_2} \right) + \frac{v_2}{\beta_2} + \frac{D_3}{v_2},$$

with $\beta_i = eE_i/m$ and

$$v_1 = \sqrt{v_z^2 + 2(D_1 - z)\beta_1},$$

$$v_2 = \sqrt{v_1^2 + 2D_2\beta_2}. \quad (1)$$

Here, we use a coordinate system whose z axis points toward the detector along the field directions. The ion of mass m is ionized at location z with the initial velocity component v_z . At the end of each field, the ion has acquired the velocities

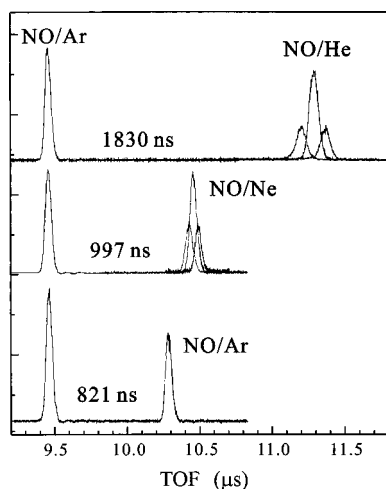


FIG. 5. TOF spectra of NO^+ for different seed conditions of NO in the indicated rare gas. In each spectrum, the early peak corresponds to NO in Ar from the primary beam source. The peak arriving at later times corresponds to NO from the target beam source.

v_1 and v_2 , respectively. Ions with the same but opposite initial velocity projections arrive with a time lag $\Delta T = 2v_z/\beta_1$ demonstrating the inverse dependence on the velocity dispersion field strength. In a typical Wiley McLaren TOF mass spectrometer, the ratio of the dispersion and acceleration fields is used to eliminate the z dependence (space focusing) of the TOF.¹⁸ On the other hand, if higher-order REMPI processes are employed for the detection, the laser beam must be focused resulting in an ionization region with an extension of less than 100 μm in the field direction and excellent velocity resolution can be achieved without meeting the space focusing condition.

III. MOLECULAR-BEAM CHARACTERISTICS

The velocity dispersion capability of the two-field/two-mirror setup is tested by expanding different NO/rare gas mixtures from both molecular-beam sources. Typical TOF spectra using (2+1) REMPI of NO are displayed in Fig. 5. In these experiments, the primary beam source (home built piezoelectric valve)¹⁹ is operated with a mixture of 5% NO in Ar. For the bottom spectrum, the target beam source (Jordan Co.) is operated with the same gas mixture. The other spectra are taken after exposing the target beam source briefly to the NO/Ar mixture, evacuating the gas inlet system and finally operating the source with the indicated rare gas. In this way, the rare gas contains only a trace amount of NO whose velocity represents, to a good approximation, the corresponding rare gas velocity. Because of the low NO concentrations, these spectra are measured with increased laser power, but under imaging conditions identical to the ones used for detecting NO from the primary beam. In all cases, the TOF peaks associated with beam pulses from both sources are narrow but significantly displaced. For the bottom spectrum, the peaks represent a velocity difference of roughly 1220 m/s which results in a TOF peak displacement of 821 ns. The measured spectra are consistent with velocities of 840 m/s

for the Ne and 1860 m/s for the He expansions. Because of the large mass difference between NO and He, the actual He velocity might be slightly larger.

It is important to realize that these TOF spectra represent the local velocity distribution within a molecular-beam pulse. Through the variation of the time delay between the pulse and the laser firing, we can measure changes of the velocity distribution throughout the pulse. Obviously, as the pulse travels away from the molecular-beam source, the different velocity subgroups separate resulting in fast molecules arriving first at the laser detection volume. Experimentally, we observe the variation of the TOF peak position and width as a function of the relative delay. Expanding a mixture of 5% NO in Ar from both molecular-beam sources, we find similar peak intensities and pulse durations. On the other hand, the TOF peak positions corresponding to the full width at half maximum (FWHM) delays vary 27 ns for the piezoelectric valve and 71 ns for the Jordan beam source. For the expansion of trace amounts of NO in Ne or He from the Jordan valve, Fig. 5 shows additional TOF spectra measured at delays corresponding to the FWHM delays. In the case of NO/He, the peak position varies by more than 170 ns which must be compared with the peak width of about 65 ns.

The TOF spectra measured at different molecular-beam delays provide information about the local width of the velocity distribution while the peak positions reflect the most probable velocity at the delay probed. Obviously, the variation of the most probable local velocity must reflect the initial velocity distribution in the pulse while the measured pulse duration can be significantly influenced by the initial velocity spread. The evolution of the velocity distribution within the molecular-beam pulse can be rationalized if we assume that, as a result of the jet expansion, a molecular-beam pulse with a homogenous velocity distribution is generated. For simplicity, we assume the intensity and velocity distributions to be of a Gaussian form with widths Δz_0 and Δv_0 :

$$F(z, v, t=0) = F_0 e^{-(z/\Delta z_0)^2} e^{-((v-v_0)/\Delta v_0)^2}. \quad (2)$$

If we probe the pulse at location \bar{z} at time $t > 0$, only a sub-ensemble of the original pulse is probed. In particular, only those molecules contribute which at $t=0$ were located at position z with a speed $v = (\bar{z} - z)/t$. Therefore, the distribution of molecules at the position \bar{z} is determined from the expression

$$F(\bar{z}, v, t) = F_0 e^{-((\bar{z}-vt)/\Delta z_0)^2} e^{-((v-v_0)/\Delta v_0)^2}. \quad (3)$$

Equation (3) can be cast into a form which directly reflects the experimentally determined local average velocity $\bar{v}(\bar{z}, t)$ and width $\Delta \bar{v}(\bar{z}, t)$:

$$F(\bar{z}, v, t) = F_0 e^{-((\bar{z}-v_0t)/\Delta \bar{z})^2} e^{-((v-\bar{v})/\Delta \bar{v})^2}. \quad (4)$$

Here, we have introduced the parameters:

TABLE I. Duration Δt in μs , velocity spread $\Delta\bar{v}$, and average velocity ν_0 measured for different molecular-beam pulses using electric fields of 4.5 V/cm and 72 V/cm for dispersion and acceleration, respectively. \bar{v}_1 and \bar{v}_2 are the average velocities measured at the FWHM delays of the pulses. The sources are labeled with P for the piezoelectric source and J for the Jordan source. Parameters $\nu_0(\text{calc})$, $\Delta\nu_0$, and Δz_0 are calculated for the initial beam pulses using a source-to-laser distance of 200 mm as described in the text. The second entry for the He beam expansion marked with an asterisk is calculated for a distance of 540 mm. Velocities are given in m/s and distances in mm.

Source	Sd	Δt	$\Delta\bar{v}$	\bar{v}_1, \bar{v}_2	ν_0	$\nu_0(\text{calc})$	$\Delta\nu_0$	Δz_0
P	Ar	60	65	600,635	610	608	64	33
J	Ar	75	80	575,655	614	614	106	30
J	Ne	65	80	800,880	840	834	115	25
J	He	45	90	1735,1930	1860	1211	237	16
J	He*					1862	237	28

$$\Delta\bar{v} = \Delta\nu_0 \frac{1}{\sqrt{1 + \alpha t^2}} \quad \text{and} \quad \bar{v} = \nu_0 \frac{1 + \alpha \bar{t}}{1 + \alpha t^2} \quad (5)$$

$$\text{with } \bar{t} = \frac{\bar{z}}{\nu_0} \quad \text{and} \quad \alpha = \left(\frac{\Delta\nu_0}{\Delta z_0} \right)^2.$$

If the pulse is probed before its maximum has reached the laser detection region ($t < \bar{t}$), a velocity distribution with an average velocity \bar{v} larger than ν_0 is found. It is also evident from Eq. (5) that the local velocity distribution narrows with travel time while the pulse spreads in space. The spatial distribution of the pulse at time t is characterized by the width $\Delta\bar{z}$:

$$\Delta\bar{z} = \Delta z_0 \sqrt{1 + \alpha t^2}. \quad (6)$$

As expected, the width of the intensity distribution is composed of contributions due to the original spatial width Δz_0 and velocity spread $\Delta\nu_0$. Experimentally, we measure the intensity profile as a function of the time delay between the laser and the molecular-beam pulse. For $(\Delta\nu_0)^2 \ll \nu_0^2$, the duration of the pulse [defined as the temporal width (FWHM)] at the position \bar{z} can be approximated as

$$\Delta t = \frac{\Delta z_0}{\nu_0} \sqrt{1 + \alpha \bar{t}^2}. \quad (7)$$

For $t \gg \Delta t$, Eqs. (5) and (7) are easily inverted to provide estimates for the characteristics of the initial pulse: $\Delta\nu_0$, Δz_0 , and ν_0 . As can be seen in Table I, the measured data are consistent with the assumption of a homogeneous velocity distribution throughout the initial pulse for expansion in Ne and Ar. The data for the expansion in He indicate strong deviations from this simple model. At the end of the expansion, i.e., within several nozzle diameters from the molecular-beam source, the He pulse already exhibits a strong spatial separation of the different velocity subgroups. Within the model of a homogenous velocity distribution, the observed velocity separation would require an increase in the overall travel distance from 20 cm to 54 cm.

Comparing the different contributions to the width in the TOF spectra, we note that the resulting width is controlled mainly by the velocity distribution in the beam. For example, the 5% NO/Ar mixture expanded from the piezoelectric

valve results in a TOF peak with a width of about 42 ns. A local velocity spread of around 60 m/s translates into an uncertainty of about 38 ns while the contribution due to an ionization volume of about 100 μm diameter results in an uncertainty of less than 14 ns. These data clearly demonstrate that the resolution in our setup is limited to a large extent by the velocity distribution of the molecular beams.

IV. MOLECULAR-BEAM SCATTERING

The TOF setup is tested further by studying the scattering of NO from Ne in a counterpropagating pulsed molecular-beam experiment. The NO beam is generated by expanding a 5% NO/Ar mixture from the piezoelectric valve at a backing pressure of 1.4 bar. The target beam is generated by expanding Ne from the Jordan valve at a backing pressure of 1.6 bar. The beam pulses have a duration of about 60 μs and 65 μs , respectively. The expansion of NO in Ar results in a rotational temperature of about 1 K consistent with the almost exclusive population of the $J_i=0.5$ level. The next higher-energy level corresponding to $J=1.5$ is reduced in intensity by a factor of at least 35. The most probable velocities in the beams are 610 m/s for NO in Ar and 840 m/s for the Ne beam, resulting in a collision energy of $(1055 \pm 75) \text{ cm}^{-1}$. TOF spectra for the different final states of NO are measured in the velocity dispersion mode described above. Most of the states probed show a small but significant rest population due to the incomplete rotational cooling of the gas mixture in the expansion. In order to distinguish the rest population from the scattering signal, we determine the difference of two TOF spectra: One measured with the target beam overlapping and one with the target beam missing the NO beam pulse. For the analysis, we also take into account the small depletion of the rest population. Depending on the spectroscopic detection scheme employed, the TOF spectra for scattering can be sensitive to the collision-induced alignment. In this case, we measure four TOF spectra: Scattering and background spectra for two different laser polarizations, either parallel or perpendicular to the molecular-beam axis. Ideally, these spectra should be determined on a shot-to-shot basis. In practice, we average 400–500 shots with a digital storage oscilloscope for a particular setting of the target beam delay and the laser polarization. The acquired spectrum is transferred to a personal computer (PC) where it is stored for further processing. Spectra for the other settings are measured in an analogous way. As a result, we build up different TOF spectra in the PC almost simultaneously avoiding the influence of long-term drift effects, e.g., in the laser power or the molecular-beam densities. After each cycle of the data acquisition, we generate TOF spectra representing the monopole and quadrupole moments in order to judge the quality of the polarization effect on the data.

Because the TOF spectra represent one-dimensional projections of the final velocity distribution onto the molecular-beam axis, the width of the distribution directly reflects the radius of the Newton sphere in velocity space. As we noted in Sec. III, the average velocity changes throughout the molecular pulse. The scattered flux detected in the TOF spectrum is typically generated in the vicinity of the laser vol-

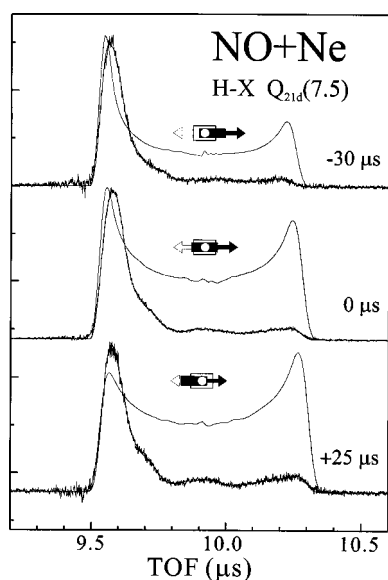


FIG. 6. TOF spectra for the scattering of NO from Ne for different delays of the target beam recorded with the laser polarized parallel to the molecular-beam axis. The direction and overlap of the primary beam (open rectangle) and the target beam (solid rectangle) pulses are indicated schematically for each delay. The solid line represents the integrated apparatus function assuming a constant differential cross section.

ume. Monte Carlo simulations of the scattering kinematics indicate that the scattered flux contributing to a TOF spectrum is generated in a region corresponding to travel times of less than $10 \mu\text{s}$. This must be compared to the pulse duration of about $60 \mu\text{s}$. By varying the target beam delay over the half width, we effectively change the average velocity of the target beam. In the case of scattering from Ne, these changes in the local velocity distribution become noticeable if TOF spectra for a particular final quantum state are measured for different molecular-beam delays. As an example, we display in Fig. 6 TOF spectra for the scattering of NO into the final state ($X^2\Pi_{1/2}, J_f = 7.5$). We employ (2+1) REMPI via the H state of NO.^{20,21} The center spectrum is measured for delays at which the maximum of each pulse reaches the laser probe volume simultaneously with the firing of the laser. For the bottom spectrum, the target beam delay is chosen in such a way that scattering involves preferentially atoms from the beginning of the target pulse. For these delays, the local Ne velocity varies from 880 m/s (large delay, bottom spectrum) to 840 m/s (maximum, center spectrum), and 800 m/s (small delay, top spectrum). Due to these changes in the average velocity, the size of the Newton sphere varies accordingly as can be seen in Fig. 6.

Obviously, for different delays of the target beam, the two molecular-beam pulses overlap in different locations relative to the fixed laser position. If the laser is fired after the maximum of the target beam has reached the detection volume, scattered flux contributing to the TOF spectrum is generated from a region closer to the NO beam source resulting in preferential forward scattering. This is observed in the top spectrum in Fig. 6. On the other hand, if the delay for the target beam is chosen so that scattering results from the region closer to the target beam source (see bottom spectrum in Fig. 6), we observe preferential backward scattering. Apart

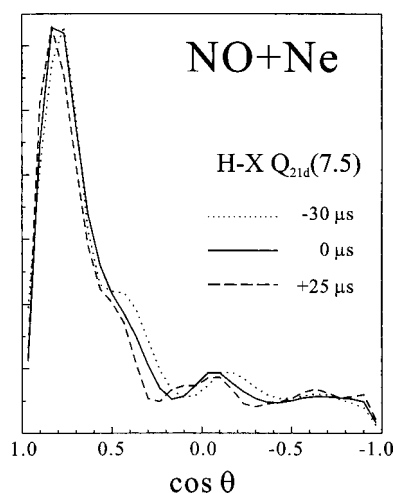


FIG. 7. Degeneracy averaged differential cross sections for the indicated final state extracted from the TOF spectra displayed in Fig. 6. Changes in the target beam delay result in small variations of the cm collision energy: 997 (dotted), 1055 (solid), and 1114 (dashed) cm^{-1} .

from the variation of the differential scattering cross section with collision energy, it must be independent of the chosen target beam delay. As shown previously, the TOF spectra can be analyzed with the help of an apparatus function describing the probability for contributions with specific velocity projections and scattering angles.^{15,17} It is calculated from the intensity and velocity distribution of the beam pulses for the appropriate delays. It also incorporates the correct scattering kinematics as well as the flux-to-density transformation. For a given differential cross section, a TOF spectrum can be predicted by convoluting the angle dependent cross section with the apparatus function. Alternatively, the differential cross section can be extracted from the measured TOF spectra in a linear least-squares fitting procedure. Neglecting small changes in the collision energy, the extracted cross section must be independent of the relative beam delays. Therefore, any delay dependence observed in the TOF spectra must be accounted for by the delay dependence of the apparatus function. That this is indeed the case can be seen in Fig. 6 where the solid lines represent the apparatus functions calculated for the appropriate delays and integrated over the scattering angle. The variation of the apparatus function with target beam delay reflects the change in detection sensitivity from forward scattering (top spectrum) to backward scattering (bottom spectrum). The differential cross sections extracted from the spectra in Fig. 6 are displayed in Fig. 7. Within the error limits, all spectra result in similar differential cross sections. Most importantly, the structures assigned as rotational rainbows are consistent for all three TOF spectra. Small variations in the positions of these structures most likely reflect the corresponding variation in the collision energy.²²

ACKNOWLEDGMENTS

Financial support provided by the National Science Foundation (Grant No. CHE-0097189) and the donors of The Petroleum Research Fund administered by the ACS is grate-

fully acknowledged. Two of the author (S. A. and B. Z.) acknowledge support from the National Science Foundation REU program (Grant No. PHY-0097457).

¹*Atomic and Molecular Beam Methods*, edited by G. Scoles (Oxford University Press, London, 1988), Vol. I.

²R. D. Levine and R. B. Bernstein, *Molecular Reaction Dynamics and Chemical Reactivity* (Oxford University Press, Oxford, 1987).

³*Atomic and Molecular Beams: The State of the Art 2000*, edited by R. D. Campargue (Springer, Berlin, 2001).

⁴L. Schnieder, K. Seekamp-Rahn, F. Liedeker, H. Steuwe, and K. Welge, *Faraday Discuss. Chem. Soc.* **91**, 259 (1991).

⁵S. D. Chao, S. A. Harich, D. X. Dai, C. C. Wang, X. Yang, and R. T. Skodje, *J. Chem. Phys.* **117**, 8341 (2002).

⁶R. L. Miller, S. H. Kable, P. L. Houston, and I. Burak, *J. Chem. Phys.* **96**, 332 (1992).

⁷S. Klee, K. H. Gericke, and F. J. Comes, *J. Chem. Phys.* **85**, 40 (1986).

⁸M. Dubs, U. Bruhlmann, and J. R. Huber, *J. Chem. Phys.* **84**, 3106 (1986).

⁹D. W. Chandler and P. L. Houston, *J. Chem. Phys.* **87**, 1445 (1987).

¹⁰L. S. Bontuyan, A. Suits, P. L. Houston, and B. J. Whitaker, *J. Phys. Chem.* **97**, 6342 (1993).

¹¹N. Yonekura, C. Gebauer, H. Kohguchi, and T. Suzuki, *Rev. Sci. Instrum.* **70**, 3265 (1999).

¹²A. G. Suits, L. S. Bontuyan, P. L. Houston, and B. J. Whitaker, *J. Chem. Phys.* **96**, 8618 (1992).

¹³W. R. Simpson, A. J. Orr-Ewing, T. P. Rakitzis, S. A. Kandel, and R. N. Zare, *J. Chem. Phys.* **103**, 7299 (1995).

¹⁴L. H. Lai, J. H. Wang, D. C. Che, and K. Liu, *J. Chem. Phys.* **105**, 3332 (1996).

¹⁵H. Meyer, in *Atomic and Molecular Beams: The State of the Art 2000*, edited by R. D. Campargue (Springer, New York, 2001).

¹⁶H. Meyer, *J. Chem. Phys.* **101**, 6686 (1994).

¹⁷H. Meyer, *J. Chem. Phys.* **101**, 6697 (1994).

¹⁸W. C. Wiley and I. H. McLaren, *Rev. Sci. Instrum.* **26**, 1150 (1955).

¹⁹The original piezoelectric pulsed molecular-beam valve was developed in the group of Professor D. Gerlich at the University of Chemnitz, Germany.

²⁰K. P. Huber and E. Miescher, *Helv. Phys. Acta* **36**, 257 (1963).

²¹H. Meyer, *J. Chem. Phys.* **107**, 7721 (1997).

²²M. H. Alexander, Y. Kim, and H. Meyer, *J. Chem. Phys.* (submitted).